The Distance to the Sagittarius Dwarf Galaxy and its relation to M54 using Infrared Photometry of RR Lyrae Variable Stars

Arvind F. Gupta

May 11, 2018

Department of Astronomy

University of Virginia

Instructor: Steve Majewski

This thesis is submitted in partial completion of the requirements of the

BS Astronomy-Physics Major at the University of Virginia

Abstract

The Sagittarius dwarf galaxy (Sgr) is among the most massive satellites of the Milky Way and is unique due to its extensive tails of tidally stripped stars. Models of these tails provide strong constraints on the orbital history of Sgr, which in turn lend insight into the structure of the Milky Way's dark matter halo. Fully understanding the dynamics of Sgr, however, relies on a precise distance to the core. Yet past measurements yield a wide range of values (22.0 - 28.4 kpc) or a variation of $\sim 25\%$. In addition, the line-of-sight separation of Sgr from the globular cluster M 54 is an important test of the "cusp-core problem", which highlights the discrepancy between expected formation scenarios for dwarf galaxy dark matter haloes and their observed density distributions.

Through photometry of 3.6μm *Spitzer* IRAC data and GLOESS light curve fitting, we have measured the mean apparent magnitudes of 45 RR Lyrae variables in the Sgr core and 25 RR Lyrae stars in M 54. Apparent magnitudes are measured using multi-epoch PSF photometry, and corresponding absolute magnitudes are determined via the RR Lyrae period-luminosity relation. We find the mean distances to Sgr and M 54 to be $d_{Sgr} = 27.10 \pm 0.21$ (ran) $\pm$ 1.11 (sys) kpc and $d_{M54} = 26.42 \pm 0.34$(ran)$\pm$0.97(sys) kpc, respectively. Our result improves the precision with which the distance to Sgr is known. We also show that the separation of M 54 and Sgr indicates that the Sgr dark matter halo is presently cored, suggesting that the dwarf galaxy has undergone a cusp-core transformation.

Draft version May 4, 2018
Preprint typeset using LaTeX style emulateapj v. 12/16/11

THE DISTANCE TO THE SAGITTARIUS DWARF GALAXY AND ITS RELATION TO M54 USING INFRARED PHOTOMETRY OF RR LYRAE VARIABLE STARS

Arvind F. Gupta[1], Steven R. Majewski[1], Rachael L. Beaton[2,3]

Draft version May 4, 2018

ABSTRACT

The Sagittarius dwarf galaxy (Sgr) is among the most massive satellites of the Milky Way and is unique due to its extensive tails of tidally stripped stars. Models of these tails provide strong constraints on the orbital history of Sgr, which in turn lend insight into the structure of the Milky Way's dark matter halo. Fully understanding the dynamics of Sgr, however, relies on a precise distance to the core. Yet past measurements yield a wide range of values (22.0 - 28.4 kpc) or a variation of $\sim 25\%$. In addition, the line-of-sight separation of Sgr from the globular cluster M 54 is an important test of the "cusp-core problem", which highlights the discrepancy between expected formation scenarios for dwarf galaxy dark matter haloes and their observed density distributions.

Through photometry of 3.6μm *Spitzer* IRAC data and GLOESS light curve fitting, we have measured the mean apparent magnitudes of 45 RR Lyrae variables in the Sgr core and 25 RR Lyrae stars in M 54. Apparent magnitudes are measured using multi-epoch PSF photometry, and corresponding absolute magnitudes are determined via the RR Lyrae period-luminosity relation. We find the mean distances to Sgr and M 54 to be $d_{Sgr} = 27.10 \pm 0.21$ (ran) $\pm$ 1.11 (sys) kpc and $d_{M54} = 26.42 \pm 0.34$(ran)$\pm$0.97(sys) kpc, respectively. Our result improves the precision with which the distance to Sgr is known. We also show that the separation of M 54 and Sgr indicates that the Sgr dark matter halo is presently cored, suggesting that the dwarf galaxy has undergone a cusp-core transformation.

1. INTRODUCTION

The Sagittarius dwarf spheroidal galaxy (Sgr) is unique among satellites of the Milky Way for its extensive tails of tidally stripped stars. The tails, mapped 360° around the sky by Majewski et al. (2003), make the dwarf galaxy an excellent tracer of the gravitational potential that dictates its orbit—that of the dark matter-dominated Milky Way Galaxy. Whereas studies of the orbits of most dwarf galaxies, globular clusters, and other satellites are limited to the motions of the bodies themselves, the orbital history of Sgr can be further constrained by the positions and kinematics of its tidal debris. Through simulations that accurately reproduce most of the observed structure of the Sgr tails, models are thus able to constrain the three-dimensional distribution of dark matter in the Milky Way Galaxy (Law & Majewski 2010; Vera-Ciro & Helmi 2013; Ibata et al. 2013). Studies such as these, however, offer contrasting results, particularly in the axial ratios of the Milky Way dark matter halo. Whereas Law & Majewski (2010) find that the halo is triaxial, with the major axis oriented perpendicular to the Milky Way disk, Ibata et al. (2013) find the halo to be axisymmetric.

The contrasting results might, at least in part, be attributed to a sensitivity to certain input parameters. Vera-Ciro & Helmi (2013), for example, account for gravitational effects from the Large Magellanic Cloud, pointing to how this might influence the orientation of the Sgr orbit. In addition, past measurements of the distance to the core of Sgr exhibit wide variation, ranging from 22 kpc (Alcock et al. 1997) to 28.4 kpc (Siegel et al. 2007). And until the recent result of Hamanowicz et al. (2016) ($d_{Sgr} = 26.98 \pm 0.25$kpc) no measurements were much more precise than $\pm$1kpc. In simulations that assume an inaccurate Sgr core distance, the mass internal to the tails could change enough to significantly affect the inferred Milky Way matter distribution. A more precise distance determination is thus essential to our understanding of the Milky Way dark matter distribution.

The distance to the core of Sgr is also of interest given its association with the globular cluster M 54. M 54, located at (RA, Dec) = (18h55m03.33s, $-30°28'47.5"$), coincides in projected, on-sky position with the center of Sgr, suggesting that it is actually the nucleus of the dwarf galaxy (Majewski et al. 2003). The Sgr core distance upon which the Law & Majewski (2010) study relies was determined by Siegel et al. (2007) as the distance to M 54, assuming that the bodies lie at the same distance. But the two are both chemically (Siegel et al. 2007) and kinematically (Bellazzini et al. 2008) distinct and thus were unlikely to have formed co-spatially. If they presently share the same position in 3-dimensional space, M 54 must have spiralled to the center of Sgr in the thirteen billion years since its formation.

M 54 is indeed expected to have fallen into Sgr, as the orbit of the cluster should have decayed due to dynamical friction in the presence of the Sgr dark matter halo (Bellazzini et al. 2008). Yet measurements of the relative distance of M 54 and Sgr demonstrate that this is not the case. Siegel et al. (2011) find via isochrone fitting that M 54 lies 2 kpc in the foreground of Sgr. Using RR Lyrae stars found in the Optical Gravitational Lensing Experiment (OGLE), Hamanowicz et al. (2016) measure an offset as well, finding that M 54 is separated from the center of Sgr by roughly 0.5 kpc. These distance offsets

afgupta@virginia.edu
[1] The University of Virginia
[2] The Observatories of the Carnegie Institute for Science
[3] Princeton University

indicate that the Sgr dark matter halo did not form with a sharp, central cusp, as models predict, but rather with a shallower cored profile. This "cusp-core problem" was first described by Moore (1994) based on the discrepancy between observed and modeled HI velocity functions for nearby dwarf galaxies. As Moore (1994) explains, the formation of a cored halo requires the presence of warm, collisional dark matter particles, and is thus incompatible with CDM cosmology.

This cusp-core problem is also seen in the results of the Goerdt et al. (2006) study of the Fornax dwarf galaxy. Aside from Sgr, Fornax is the only Milky Way satellite known to host globular clusters. Under the influence of a cusped dark matter halo, the orbits of the five Fornax clusters are expected to have decayed, but all five still orbit at projected radii of ≈ 1 kpc. Goerdt et al. (2006) show that this lack of decay, and thus of dynamical friction, is only compatible with a cored profile. More recently, however, theoretical simulations spurred by work in this vein have shown that this discrepancy can be reconciled via stellar feedback (Mashchenko et al. 2008; Teyssier et al. 2013; Brooks et al. 2017). These studies find that feedback in the form stellar winds and supernovae can flatten out the dark matter profiles of dwarf galaxies. This mechanism of core formation is particularly effective in the $10^{10} M_{\odot}$ mass regime, where star formation rates are high enough to drive feedback (Brooks et al. 2017). The work of Goerdt et al. (2006) appears to indicate that such a cusp-core transformation has indeed occurred in Fornax. Further study of the line-of-sight distance between M 54 and Sgr will help determine whether their relation reflects that of Fornax and its satellites and shed light on the density profile of the Sgr dark matter halo.

In this work, we determine distances to M 54 and Sgr via photometry of RR Lyrae (RRL) variable stars in *Spitzer Space Telescope* data. RRL are pulsational variables, expanding and contracting due to opacity inversions in the HeII ionization layer in the stellar interior (known as the κ-mechanism), producing a periodic change in brightness. And given the well-established relation between their pulsation periods and mean absolute magnitudes, RRL can serve as powerful distance indicators for "Population II" (old, metal-poor) bodies in which they are present, such as Sgr and M 54. By photometrically measuring the apparent magnitudes of RRL with known periods, it is thus possible to determine their distances.

All past distance measurements to Sgr using RRL, however, have relied on observations at optical wavelengths. Several key advantages are conferred by working in the infrared. First, extinction due to dust can significantly compound the uncertainties on magnitudes measured at optical wavelengths. This effect is greatly reduced in the infrared, where extinction is not as strong. This is especially important given that the line of sight to M 54 and to Sgr passes close to the Galactic center. Second, the pulsation amplitudes of RRL are smaller and more sinusoidal in the infrared (as opposed to the typical sawtooth shape seen in the optical), allowing for more accurate determination of mean apparent magnitudes. Third, the period-luminosity relation for the *Spitzer* 3.6μm and 4.5μm bands has been calibrated to a high precision (Neeley et al. 2015, 2017). And finally, the period-luminosity relation exhibits a metallicity dependence that, while strong in the optical, is relatively weak in the infrared (Catelan et al. 2004; Madore et al. 2013).

In the following section, we first detail the *Spitzer* observations and the Sgr and M 54 data used in this study. In Section 3 we discuss our photometry methods and the measurement of mean apparent magnitudes for all of the target RRL, and in Section 4 we explain how we arrive at our final sample of stars following several rounds of cuts. In Section 5, we discuss the extinction correction. Sections 6 and 7 detail the distance determinations for both Sgr and M 54, as well as the consequences of those results.

2. *SPITZER* OBSERVATIONS

Observations for Sgr were made in July 2014 as part of the *Spitzer* Merger History and Shape of the Galactic Halo (SMHASH) project using the *Spitzer Space Telescope* Infrared Array Camera at 3.6μm. The positions of RRL as determined by Cseresnjes et al. (2000) in an optical study were used to select twenty pointings throughout the NW region of the Sgr core, each containing 2 to 6 RRL (Figure 1) for a total of 74 target RRL. The center coordinates of each pointing are given in Table 1. Twelve epochs of data were collected for each field, spanning 15 hours, or roughly the full pulsational period of the longest period RRL in our footprint. The epochs were evenly spaced in time such that measurements would be well sampled across the period of each target. This low cadence, with roughly 90 minute intervals between observations, is sufficient for our work given that we do not aim to search for new variable stars, nor will we attempt to determine more precise periods for known RRL. For each epoch, 10 drizzled $5.2' \times 5.2'$, 12 second exposures were taken. The individual exposures were processed and mosaicked according to standard Spitzer S19.2 procedure, producing a single $7.14' \times 8.05'$, 55 second frame for each epoch. In this step, the image resolution was also increased from 1.2" to 0.6" per pixel to combat undersampling of the stellar profiles (Scowcroft et al. 2013).

Observations for M 54 were made in a similar manner on December 2, 2012 as part of the Carnegie RR Lyrae Program (CRRP). A single pointing was selected such that M 54 was offset from the center, as shown in Figure 2, falling primarily in one half of the *Spitzer* footprint. Using positions obtained from the OGLE-IV catalog (Soszyński et al. 2014), 114 RRL were found to lie within the field of view. Twelve epochs of 3.6μm data were collected, spanning 17 hours and each consisting of 9 individual exposures. These were again processed and mosaicked according to S19.2 procedure. For each epoch, a single $7.91' \times 13.19'$ (791×1319 pixels at $0.6''$/pixel) frame with a total exposure time of 30 seconds was produced.

3. PHOTOMETRY

3.1. *Sgr*

Photometry was performed independently for each Sgr field using the DAOPHOT (Stetson 1987, 1994) software package. Through DAOPHOT, a point spread function (PSF) was fitted iteratively to bright, isolated stars free from crowding or saturation. A single PSF was constructed for each field; because all observations for a

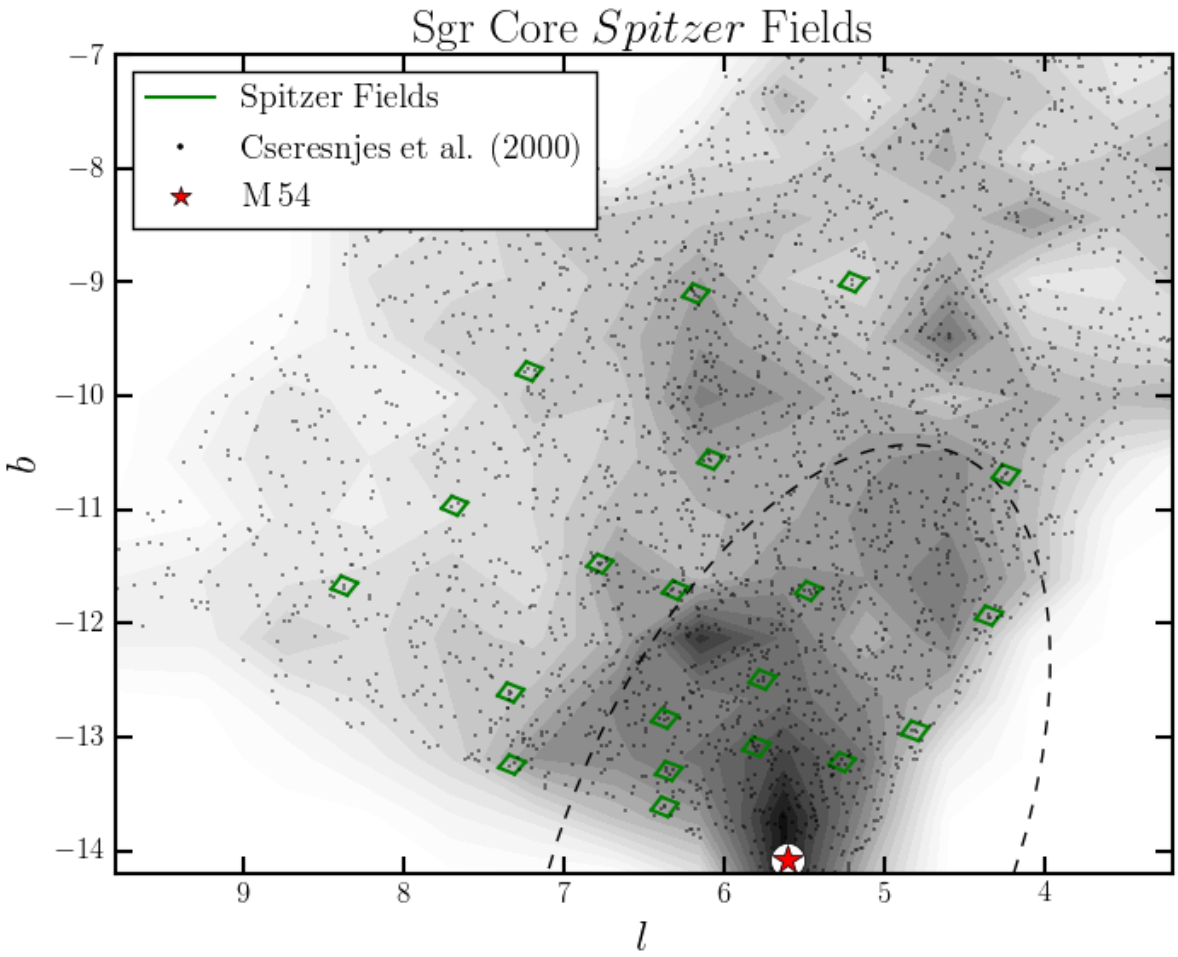

FIG. 1.— The coverage of the twenty 3.6μm *Spitzer* fields (in green) superimposed over a normalized number density contour of RR Lyrae stars in Sgr from Cseresnjes et al. (2000) restricted to B > 18.0 to avoid bulge RRL. The individual RR Lyrae stars are also displayed. The chosen fields were dispersed such that RR Lyrae at various radii from the center would be observed and measured. The position of the globular cluster M 54 is given by the red star, marking the center of the Sgr RRL surface density profile.

TABLE 1
SGR *Sptizer* POINTINGS USED IN THIS WORK

Pointing Name	R.A. (J2000)	Dec (J2000)
Pointing 1	18:48:44.88	-30:43:50.92
Pointing 2	18:43:35.84	-30:43:28.28
Pointing 3	18:50:45.14	-30:26:07.65
Pointing 4	18:38:09.89	-30:17:39.80
Pointing 5	18:51:08.88	-29:54:24.15
Pointing 6	18:48:35.85	-29:41:48.82
Pointing 7	18:44:48.03	-29:37:50.10
Pointing 8	18:54:24.93	-29:36:37.64
Pointing 9	18:53:02.90	-29:30:22.98
Pointing 10	18:51:09.88	-29:17:48.29
Pointing 11	18:46:20.09	-28:53:16.22
Pointing 12	18:33:02.83	-28:42:46.45
Pointing 13	18:54:34.91	-28:36:46.93
Pointing 14	18:41:09.83	-28:36:11.64
Pointing 15	18:46:15.17	-28:22:20.10
Pointing 16	18:51:57.90	-28:20:43.42
Pointing 17	18:35:22.90	-27:53:17.15
Pointing 18	18:45:51.17	-27:20:57.72
Pointing 19	18:40:09.90	-27:15:42.63
Pointing 20	18:49:59.92	-27:02:03.62

given field were conducted in less than a day, variation of the profile from epoch to epoch was assumed to be negligible. This was confirmed as no systematic variations were observed in star-subtracted images.

To elevate the S/N level and allow for detection of fainter sources, a median image was constructed from the 12 epochs for each field using the MONTAGE2 function in DAOPHOT. Master source catalogs were generated from the median images. The epoch to epoch position offsets were determined using DAOMATCH and DAOMASTER, and then the PSF was fit to each source using ALLFRAME, producing instrumental magnitudes for every star in the catalog.

3.2. *M54*

Each mosaicked M 54 image was first split in half, yielding pairs of "field" and "cluster" images. Initial photometry was performed on the split images using DAOPHOT (Stetson 1987). Bright, isolated sources in the less crowded field images were used to determine an empirical point spread function (PSF). Whereas the Sgr PSF was found to be insensitive to differences between epochs, variation was observed for M 54. Separate PSFs

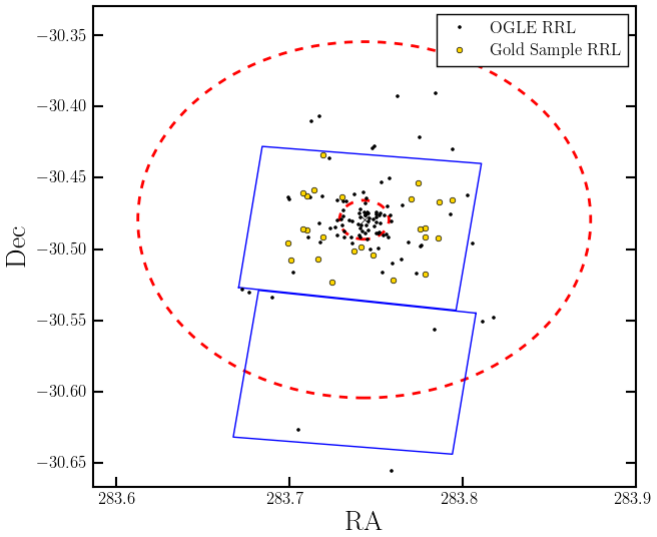

FIG. 2.— Data footprint from the *Spitzer Space Telescope* observations of M 54. The blue rectangles depict the on-sky coverage of the observations. The OGLE positions of the gold sample RRL are plotted in yellow, and all rejected candidates are shown as black points. The large and small red, dashed circles represent the tidal and half-light radii of M 54, respectively.

were thus generated for each M 54 epoch. The 12 cluster frames were then used to construct an elevated signal-to-noise median cluster image, from which a master source catalog was generated. Using ALLFRAME (Stetson 1994), instrumental photometric magnitudes were then determined for each epoch by fitting the PSFs to the detected sources in the corresponding cluster images.

3.3. *Calibration*

For both Sgr and M 54, the photometry was calibrated following the procedures outlined in Scowcroft et al. (2013) to place the magnitudes on the standard IRAC system defined by Reach et al. (2005). The output ALLFRAME magnitudes were offset against aperture photometry to which an aperture correction of 1.128 was applied. The aperture photometry was performed in DAOPHOT on the bright, isolated PSF stars in the original flux-unit images using a photometry radius of 6 pixels (3.6″) and sky annulus radii of 6 pixels (3.6″) and 14 pixels (8.4″). A magnitude offset was applied to account for the difference between the DAOPHOT system zero point of 25.00 and the IRAC 3.6μm zero point of 18.80. The final apparent magnitudes were scaled to correct for the known variation in exposure time ($< 5\%$) across each mosaicked image.

3.4. *Light Curves*

The images were examined by eye to search for any sources of contamination, such as transients and image artifacts, near the target RRL. Where contamination was apparent, data were removed from the sample. Light curves were then fit to the calibrated photometry for each of the 114 Sgr RRL and 74 M 54 RRL using the Gaussian-windowed Local Regression (GLOESS) algorithm (Persson et al. 2004; Monson et al. 2017). The GLOESS method takes the magnitude measurements and their photometric uncertainties and an input period (here we use the periods measured by Cseresnjes et al. (2000) and Soszyński et al. (2014) for the stars in Sgr and M 54, respectively) and fits a periodic curve to the individual apparent magnitude measurements, interpolating between data points and weighting each point by its uncertainties. Time-averaged mean apparent mean fluxes and corresponding mean apparent magnitudes, $m_{[3.6]}$, were calculated from the fitted curves. Uncertainties on the mean magnitudes, $\sigma_{[3.6]}$ were determined according to

$$\sigma_{[3.6]} = \sqrt{\frac{\Sigma\sigma_i^2}{N^2} + \sigma_{\rm fit}^2} \quad (1)$$

where σ_i are the photometric uncertainties for individual epochs and $\sigma_{\rm fit} = A/N\sqrt{12}$ is the uncertainty introduced by the GLOESS fit. Following Scowcroft et al. (2011), we allow $\sigma_{\rm fit}$ to fall off as $1/N$ rather than $1/\sqrt{N}$ given the even time sampling and full phase coverage of the observations.

4. COMPLETENESS AND MEMBERSHIP

Of the 74 stars in the Sgr sample, 73 are fundamental mode, RRab variables as determined by Cseresnjes et al. (2000). The remaining star is a first overtone, RRc variable. While there exists a combined period-luminosity relation that accounts for RRc stars (Neeley et al. 2015, 2017), we choose to exclude this single star to make use of the higher precision fundamental mode period-luminosity relation. From Soszyński et al. (2014), we find that 18 of the RRL in M 54 are RRc variables and 1 is a double-mode, RRd variable. To maintain consistency with the Sgr data set, we use only the 95 RRab stars in our analysis of M 54. The GLOESS-fitted light curves were then used to refine the remaining samples of RRab stars.

In examining the photometry and fitted light curves, we find that many of the M 54 RRL close to the center of the cluster show little to no brightness variation. This is indicative of blending, in which the PSFs of the RRL are not accurately separated from those of neighboring (and often overlapping) stars, resulting in the measurement of excess flux and an elevated base brightness level. In addition, many stars that do show variation also have very large uncertainties on individual magnitude measurements. A total of 65 blended and noise-dominated RRL were removed from our sample. While the level of crowding in the Sgr fields is much lower than that of M 54, we see similar effects for 21 Sgr RRL, and these are removed as well.

Finally, we look at several M 54 stars that exhibit atypical light curves. The first of these is OGLE 37547, for which we see a small dip at peak brightness that is repeated over two periods. This dip is not present in the OGLE I-band light curves, and we see nothing in the *Spitzer* images to which it might be attributed. Nevertheless, we choose to exclude this star from our sample as it might skew the mean magnitude calculation. Three other stars with otherwise clean photometry, OGLE 37514, OGLE 37553, and OGLE 37617, have several magnitude measurements that deviate from the expected light curve. These RRL are removed from the sample as well.

4.1. *Membership*

Not all of the RRL within the *Spitzer* footprint are necessarily members of M 54 or Sgr. Seven Sgr RRL were found to be foreground stars on the basis of their brightnesses and were removed. The B magnitudes of these star in the Cseresnjes et al. (2000) catalog were checked and found to be consistent with the foreground Milky Way population. For M 54, we impose a conservative magnitude cutoff of $m_{[3.6]} = 15.50$ to remove foreground RRL from our sample. Only one star with a good light curve and magnitude measurements, OGLE 37635, is brighter than this cutoff value. This is consistent with the findings of Hamanowicz et al. (2016), which also place OGLE 37635 in the foreground. We do acknowledge that other foreground RRab stars might lie in our data footprint, but that these may not have survived the initial quality cuts resulting from crowding. We are then left with 45 Sgr RRL and 25 M 54 RRL for our final "gold sample."

Given that M 54 coincides in on-sky position with Sgr, we cannot entirely rule out the possibility that several of the RRL in the cluster images are not in fact members of M 54 but rather of Sgr. We cannot make any definitive cuts, however, without making assumptions about the differences between the two bodies. We account for this by examining the radial RRL surface density profile of Sgr. Cseresnjes et al. (2000) fit four models (King, exponential, Gaussian, and linear) to a map of the 1500 Sgr RRL detected in their study. From these model fits, we determine that between 4 and 8 RRL between the M 54 half-light and tidal radii are likely members of Sgr. Further, within the more restricted 1' to 3' region occupied by our M 54 gold sample, no more than 1 star is expected to belong to Sgr. As we cannot determine which star this might be, we do not reclassify any of the RRL. The observed properties of the gold sample stars are summarized in Tables 2 and 3 for Sgr and M 54, respectively. Light curves for the gold sample Sgr RRL are presented in Figures 3 and 4. Light curves for the gold sample M 54 RRL are shown in Figure 5, and for several of the rejected M 54 stars in Figure 6.

5. EXTINCTION

The line of sight to Sgr passes very close to the Galactic plane ($-9^\circ > b > -14^\circ$), leading . While this is often a strong limiting factor on the precision of optical measurements, observational studies in the infrared are much less sensitive to dust. Assuming a reddening law of $R_V = 3.1$, the extinction at 3.6μm is given as $A_{[3/6]}/A_V = 0.064$ (Indebetouw et al. 2005).

For each RRL in the gold sample, the line of sight reddening was obtained from the Schlegel et al. (1998) dust maps and normalized according to Schlafly & Finkbeiner (2011). Again taking $R_V = 3.1$, we then determine A_V and $A_{[3.6]}$ for each target star and calculate extinction-corrected mean apparent magnitudes. Extinction values for the Sgr RRL spanned from $A_{[3.6]} = 0.024 \pm 0.005$ mag to $A_{[3.6]} = 0.054 \pm 0.009$ mag over our imaging footprint (Figure 1). The extinction corrections for all of the M 54 RRL studied in this work were $A_{[3.6]} = 0.026$ mag, with uncertainties of ± 0.005 mag and varying by $< 0.5\%$ with position.

6. THE DISTANCE TO SGR

Extinction-corrected mean apparent magnitude were plotted against $\log(P)$ for each of the Sgr RRL (Figure 7). Corresponding absolute magnitudes were calculated according to the 3.6μm period-luminosity relation

$$m_{[3.6]} = -2.342(\pm 0.140)\log(P) - 1.155(\pm 0.089) \quad (2)$$

(Neeley et al. 2017). The slope of the period-luminosity relation was fit by Neeley et al. (2015) using RRL in the nearby globular cluster M 4, and the zero point is based off of Hubble Space Telescope parallax measurements of 5 Galactic RRL (Benedict et al. 2011). The distance modulus for each star was calculated and the mean distance modulus to the dwarf galaxy was found to be $\mu = 17.165 \pm 0.017$ (ran) $\pm$ 0.080 (sys), yielding a distance of $d_{Sgr} = 27.10 \pm 0.21$ (ran) $\pm$ 1.11 (sys) kpc.

6.1. *Past Distance Measurements*

A summary of several past distance measurements to Sgr is given in Table 4. Several of the earliest measurements (Mateo et al. 1995, 1996; Alard 1996; Alcock et al. 1997) make use of optical data of just a few RRL scattered throughout the body of Sgr. Though our findings are consistent with Mateo et al. (1995) and Mateo et al. (1996), it is difficult to draw any conclusions given their large uncertainties. We note that we are also consistent with the results of Bellazzini et al. (1999) via horizontal branch fitting and Monaco et al. (2004) via tip of the red giant branch fitting, though these measurements are also accompanied by large uncertainties. We find it promising that our result is consistent with that of Hamanowicz et al. (2016), the most precise measurement to date, which uses RRL along the same general line of sight. Though OGLE operated in the optical, their sample size and number of observations per star were each an order of magnitude larger than ours, driving their uncertainty down to the same level as that of this study.

Two other Sgr distance measurements, those of Layden & Sarajedini (2000) and Siegel et al. (2007), are in fact measurements of the distance to M 54. These studies assume that M 54 is currently in the center of Sgr. We discuss the separation further in the following section, but it important to note that it is still in question.

6.2. *Sgr Structure and Line-of-sight Depth*

The uncertainties on individual RRL mean magnitude measurements are small enough (0.14 - 0.29) that we may be able to learn more about the core of Sgr than simply its mean distance. By examining the magnitude residuals of the RRL about the period-luminosity relation, the line-of-sight extension of the core can be determined. While the metallicity dependence of the period-luminosity relation is expected to contribute to some of this scatter, the dependence is small enough at 3.6μm that it cannot account for the entire observed depth. As shown in Figure 8, the core is several kiloparsecs deep along the line of sight. This is consistent with the analysis if Hamanowicz et al. (2016), in which the FWHM of the core was found to be 2.49 kpc.

To understand the full three-dimensional shape of the core, we need to study the spatial dependence of the Sgr line of sight depth. Knowing the shape of the core is necessary for understanding the distribution of mass in Sgr, as well as for ascertaining the morphological nature

TABLE 2
Mean Magnitudes for Sgr RRab in this Work

Star ID[a]	Coordinates[a]		P^a	[3.6]	$e_{[3.6]}$	$a_{[3.6]}$	$A^b_{[3.6]}$	Notes
	R.A.	Dec	[day]	[mag]	[mag]	[mag]	[mag]	
vs1f250	18:48:47.2	-30:42:28.0	0.65805	16.486	0.010	0.283	0.030	Contamination in Epoch 4
vs5f251	18:48:43.0	-30:43:36.8	0.58950	16.454	0.008	0.221	0.030	
vs6f251	18:48:44.1	-30:44:33.5	0.48447	16.859	0.009	0.285	0.03	
vs5f391	18:43:38.4	-30:43:57.1	0.61534	16.521	0.007	0.182	0.025	
vs8f390	18:43:40.7	-30:43:44.4	0.59740	16.649	0.009	0.259	0.025	
vs9f390	18:43:31.9	-30:42:38.0	0.68618	16.369	0.007	0.196	0.025	
vs5f584	18:38:03.9	-30:17:29.9	0.61643	16.391	0.011	0.208	0.027	
vs8f556	18:38:18.2	-30:17:16.9	0.53452	16.712	0.011	0.274	0.026	Contamination in Epoch 7
vs0f162	18:51:17.1	-29:55:31.9	0.52990	16.672	0.011	0.207	0.028	
vs6f162	18:51:10.8	-29:53:40.6	0.51796	16.713	0.012	0.299	0.028	
vs7f162	18:51:08.9	-29:53:09.6	0.63430	16.422	0.008	0.217	0.028	
vs8f162	18:51:06.8	-29:55:03.0	0.56197	16.721	0.013	0.251	0.028	
vs9f162	18:51:01.9	-29:52:33.1	0.66094	16.572	0.010	0.231	0.028	
vs4f245	18:48:36.5	-29:42:35.3	0.57466	16.671	0.009	0.300	0.034	
vs0f245	18:48:40.0	-29:40:53.7	0.47876	16.899	0.011	0.273	0.032	
vs5f49	18:54:24.3	-29:36:31.2	0.63644	16.510	0.012	0.278	0.030	
vs8f49	18:54:20.9	-29:36:28.6	0.60853	16.722	0.014	0.262	0.03	
vs4f49	18:54:32.3	-29:35:45.7	0.61617	16.219	0.010	0.212	0.030	
vs2f104	18:53:07.5	-29:29:28.3	0.62754	16.511	0.009	0.276	0.029	
vs13f104	18:52:56.8	-29:31:09.7	0.46549	16.915	0.008	0.226	0.029	
vs5f159	18:51:08.6	-29:18:49.7	0.63750	16.600	0.009	0.153	0.029	
vs4f159	18:51:12.8	-29:17:44.7	0.59520	16.552	0.009	0.191	0.029	
vs8f716	18:33:07.7	-28:43:10.2	0.53860	16.878	0.011	0.226	0.054	
vs2f744	18:32:58.5	-28:42:02.3	0.54261	16.528	0.013	0.207	0.055	
vs2f44	18:54:38.9	-28:36:07.6	0.50634	16.769	0.011	0.287	0.032	

[a] Adopted from Cseresnjes et al. (2000)
[b] Determined at the position of the star using Schlegel et al. (1998) and Schlafly & Finkbeiner (2011)

TABLE 3
Mean Magnitudes for M 54 RRab in this Work

Star ID[a]	Coordinates[a]		P^a	[3.6]	$e_{[3.6]}$	$a_{[3.6]}$	Notes
	R.A.	Dec	[day]	[mag]	[mag]	[mag]	
OGLE 37516	283.71508	-30.46592	0.59000070	16.484	0.010	0.241	
OGLE 37518	283.72179	-30.46697	0.57909798	16.576	0.010	0.312	
OGLE 37519	283.72267	-30.49244	0.58972767	16.524	0.010	0.221	
OGLE 37524	283.72954	-30.49189	0.57690445	16.716	0.015	0.321	
OGLE 37525	283.72967	-30.51794	0.63577385	16.409	0.011	0.161	
OGLE 37526	283.73004	-30.48592	0.60205529	16.148	0.011	0.181	
OGLE 37529	283.73242	-30.48608	0.70699678	16.318	0.012	0.346	
OGLE 37531	283.73383	-30.45397	0.61356767	16.556	0.014	0.316	
OGLE 37533	283.73779	-30.46506	0.52673059	16.790	0.013	0.257	
OGLE 37541	283.74737	-30.52197	0.50340169	16.910	0.014	0.304	
OGLE 37569	283.75850	-30.50453	0.52049875	16.579	0.011	0.200	
OGLE 37589	283.76496	-30.49872	0.74191497	16.210	0.013	0.129	
OGLE 37599	283.76892	-30.50147	0.61777335	16.231	0.016	0.275	
OGLE 37613	283.77542	-30.46361	0.73354843	16.165	0.013	0.169	
OGLE 37620	283.78108	-30.52328	0.59261686	16.526	0.011	0.284	
OGLE 37623	283.78604	-30.43414	0.51305173	16.886	0.018	0.369	
OGLE 37624	283.78608	-30.49206	0.58373598	16.663	0.019	0.203	
OGLE 37631	283.78912	-30.50728	0.49109134	16.497	0.016	0.272	
OGLE 37632	283.79092	-30.45883	0.64932137	16.569	0.010	0.209	Contamination in Epoch 6
OGLE 37637	283.79492	-30.48686	0.62438781	16.352	0.011	0.236	
OGLE 37638	283.79517	-30.46322	0.73622322	16.406	0.020	0.308	
OGLE 37640	283.79717	-30.46131	0.56416137	16.533	0.012	0.211	
OGLE 37641	283.79729	-30.48628	0.55507571	16.639	0.015	0.248	
OGLE 37646	283.80367	-30.50797	0.48877567	16.722	0.022	0.357	
OGLE 37649	283.80537	-30.49628	0.58687146	16.403	0.008	0.207	

[a] Adopted from Soszyński et al. (2014)

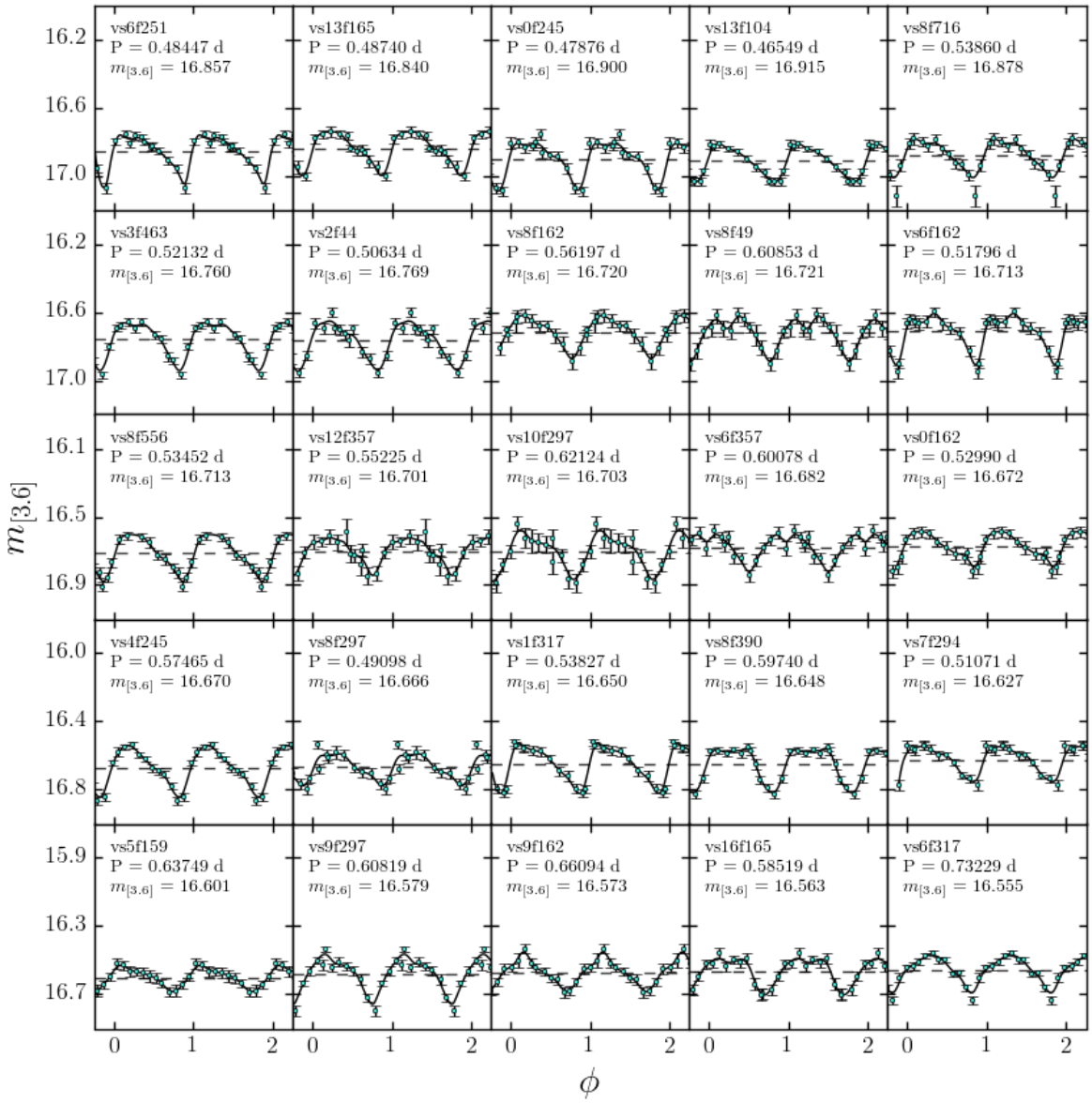

FIG. 3.— Phased light curves for 25 of the 45 RRL in our Sgr gold sample. Individual, epoch-by-epoch magnitude measurements are shown as cyan points with photometric uncertainties. GLOESS-fitted light curves are shown as a solid black line in each panel, and a dashed horizontal line indicates the time-averaged mean magnitude for each star.

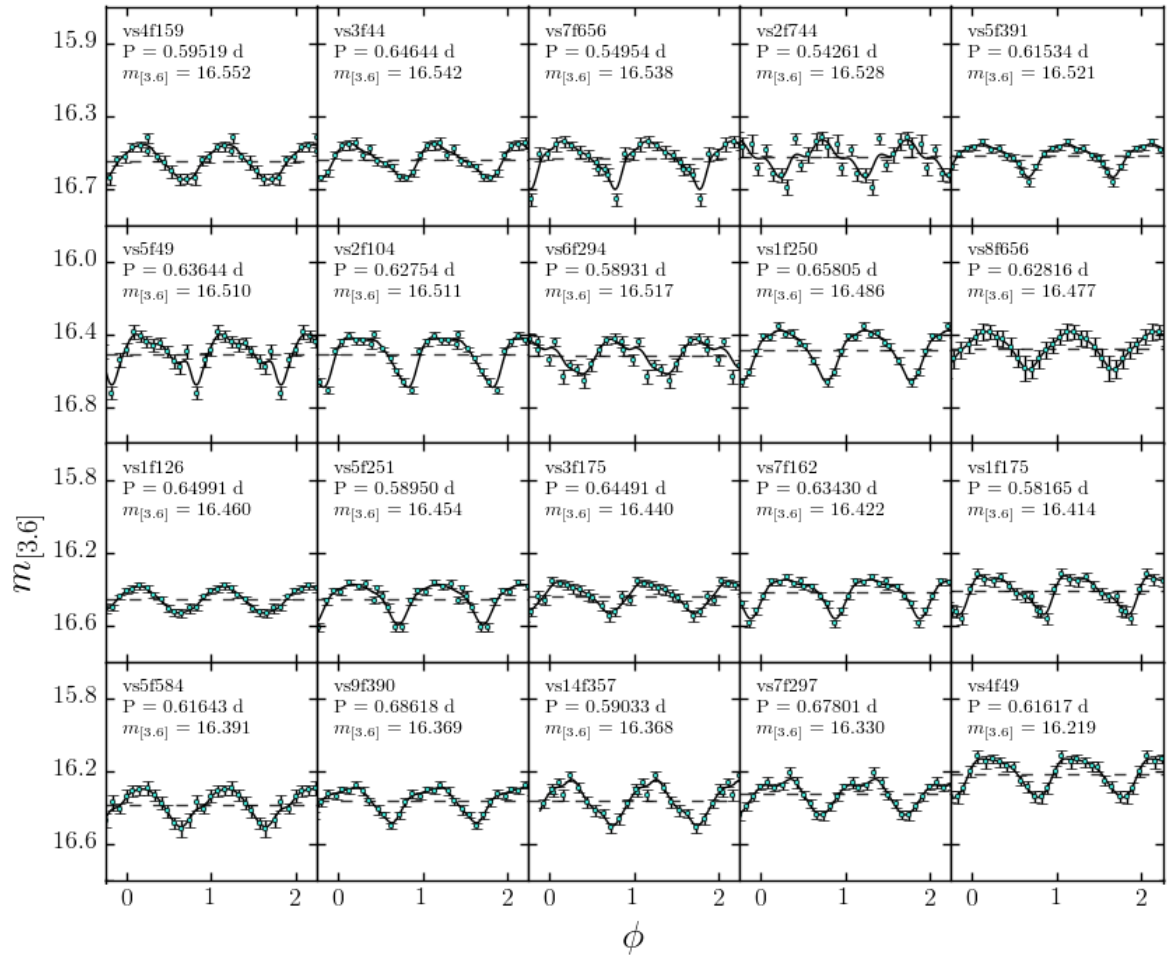

FIG. 4.— Phased light curves for 20 of the 45 RRL in our Sgr gold sample. Individual, epoch-by-epoch magnitude measurements are shown as cyan points with photometric uncertainties. GLOESS-fitted light curves are shown as a solid black line in each panel, and a dashed horizontal line indicates the time-averaged mean magnitude for each star.

TABLE 4
PAST DISTANCE MEASUREMNTS TO SGR

Method	D (kpc)	σ_D (kpc)	Reference
RR Lyrae	25.2	2.8	Mateo et al. (1995)
RR Lyrae	27.3	1.0	Mateo et al. (1996)
RR Lyrae	24.0	2.0	Alard (1996)
RR Lyrae	22.0	1.0	Alcock et al. (1997)
HB	28.0	2.0	Bellazzini et al. (1999)
RR Lyrae†	27.4	1.5	Layden & Sarajedini (2000)
TRGB	26.3	1.8	Monaco et al. (2004)
MS†	28.4	1.0	Siegel et al. (2007)
RR Lyrae	24.8	0.8	Kunder & Chaboyer (2009)
TRGB	24.3	2.3	McDonald et al. (2013)
RR Lyrae	26.98	0.25	Hamanowicz et al. (2016)

†Distance measured to M 54

of the pre-disruption of the Sgr progenitor. While this is possible using solely the *Spitzer* data, we aim to achieve a more robust result by improving the coverage of the data footprint. We have conducted follow up H-band observations using the Magellan FourStar instrument to fill some of the gaps in coverage and sample regions on the other side of the core ($b < -14$). Photometric measurements for the new RRL will be calibrated against the precise distance measurement from the *Spitzer* data and a full, well-sampled and self-consistent structural map of the Sgr core can be constructed.

7. THE DISTANCE TO M54

Absolute magnitudes for the M 54 RRL were determined according to the 3.6μm period-luminosity relation (Neeley et al. 2017) and distance moduli were calculated for each star. The mean distance modulus for the cluster was calculated to be 17.109 $\pm$ 0.028(ran)$\pm$0.080(sys), corresponding to a distance of $d_{M54} = 26.42 \pm 0.34$(ran)$\pm$0.97(sys) kpc.

7.1. *Line-of-sight Separation from Sgr*

Comparing the M 54 and Sgr distance measurements, we find that the two bodies are separated by $\Delta d = 0.68 \pm 0.40$ kpc. Here, we note that the sources of systematic uncertainty are identical for both measurements,

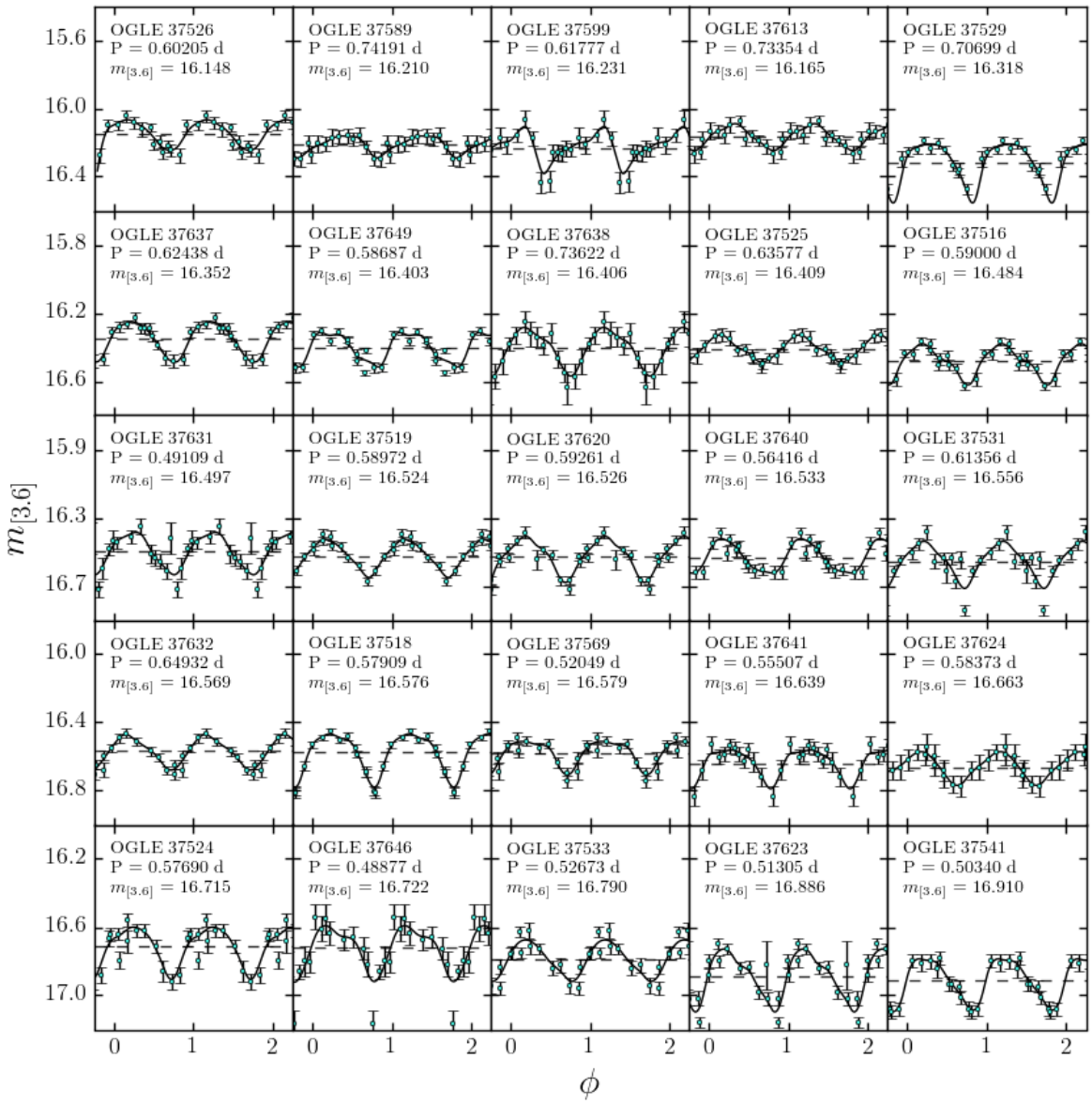

FIG. 5.— Phased light curves for the 25 RRL in our M 54 gold sample. Individual, epoch-by-epoch magnitude measurements are shown as cyan points with photometric uncertainties. GLOESS-fitted light curves are shown as a solid black line in each panel, and a dashed horizontal line indicates the time-averaged mean magnitude for each star.

so we do not factor them in to the combined uncertainty calculation. While we do find M 54 to lie in the foreground of Sgr, our result places the cluster well within the line-of-sight extension of the Sgr core. This is inconsistent with the 2 kpc offset found by Siegel et al. (2011), indicative of a cored dark matter halo for Sgr. But whereas the two bodies certainly overlap–as Figure 9 shows, the RRL occupy roughly the same region in $\log(P)$-$m_{[3.6]}$ space–there is a significant offset between their mean distances.Because our result is not consistent with an offset of zero, we cannot reconcile our findings with the presence of a cusped halo for Sgr. Still, it is unlikely that M 54 formed separately from but still within the body of Sgr. We thus expect that either (a) the orbit of M 54 partially decayed, bringing it to its current position relative to Sgr before the initial Sgr cusp was flattened out in a cusp-core transformation, or (b) Sgr formed with a cored dark matter halo and M 54 is currently passing close to the dwarf galaxy on an eccentric orbit.

We acknowledge that the distance that we measure to Sgr may not be the same as the distance to Sgr at the position of M 54, as the center of the distribution of gold sample Sgr RRL is offset from the cluster on the sky.

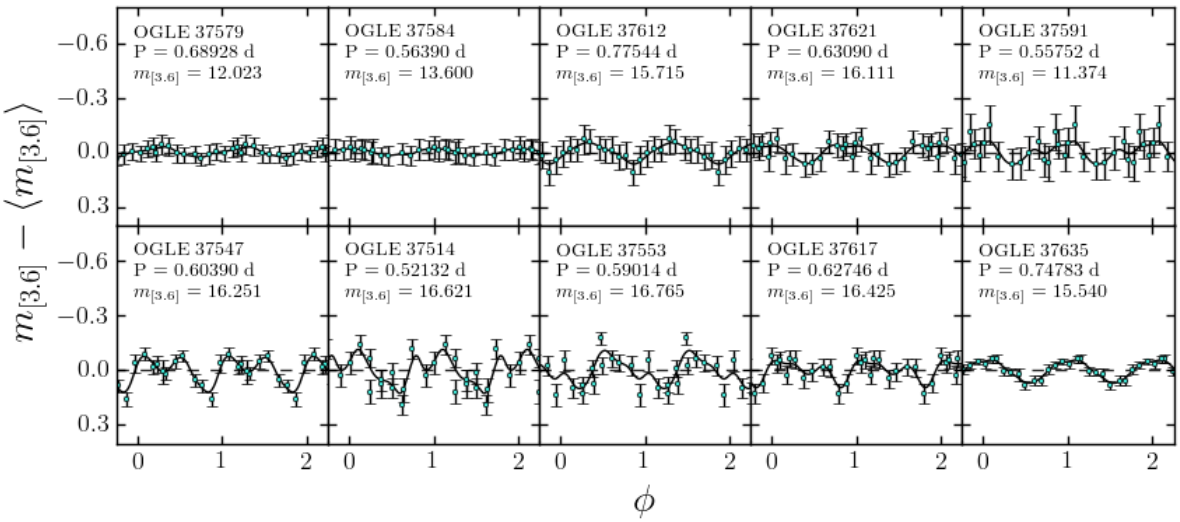

FIG. 6.— Phased light curves for the 10 of the RRab in M 54 that were removed from our sample. Individual, epoch-by-epoch magnitude measurements are shown as cyan points with photometric uncertainties. GLOESS-fitted light curves are shown as a solid black line in each panel, and a dashed horizontal line indicates the time-averaged mean magnitude for each star. The data are shifted such that the vertical axis displays the deviation from the mean magnitude for each star. The stars in the upper set of panels are lost due to crowding, as can be seen by their diminished amplitudes (OGLE 37579 and OGLE 37584) and high noise (OGLE 37612, OGLE 37621, and OGLE 37591). In the lower left panel, we show OGLE 37547, which exhibits a repeated, secondary brightness dip. The light curves for OGLE 37514, OGLE 37553, and OGLE 37617 are all relatively good but do not quite resemble what is expected for an RRL. In the lower right, we show the foreground star OGLE 37635.

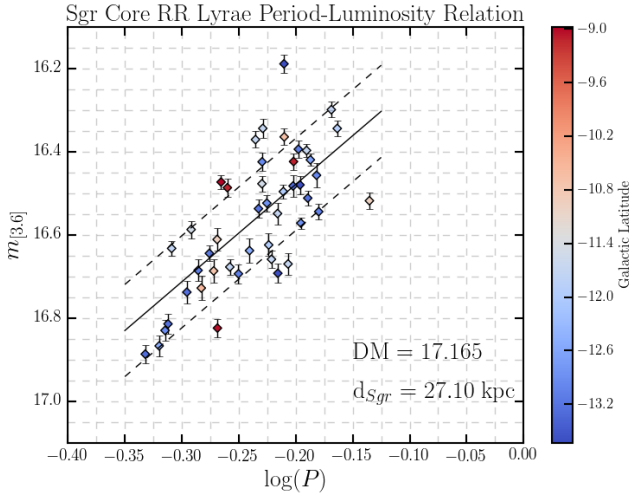

FIG. 7.— Mean apparent magnitudes for the Sgr RRL, calculated from time-average GLOESS light curves, plotted against the logarithm of the periods. Error bars indicate the uncertainty on each mean magnitude. Data points are colored by Galactic latitude, with b ranging from -13.5 (blue) to -9.0 (red). The period-luminosity relation with slope = -2.342, determined by Neeley et al. (2015) is overlaid as a solid black line. The 1σ uncertainties on the midpoint are shown as dashed black lines. The calculated distance modulus and distance are displayed in the lower right corner.

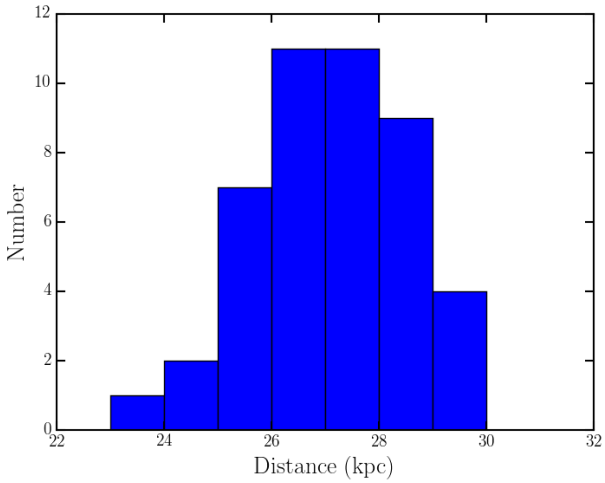

FIG. 8.— Distribution of distances measured to individual Sgr RRL in 1 kpc bins. The distribution does not quite follow a Gaussian shape as expected, but this may simply be a result of small number statistics. About 50% of stars fall within 1kpc of the calculated mean and 90% fall within 2kpc.

The idea that Sgr might have some inclination along the line of sight is discussed by Kunder & Chaboyer (2009) and Hamanowicz et al. (2016). It is possible that Sgr is inclined such that the distance offset we measure is a consequence of the surface position offset. As shown in Figure 7, however, we find no trend in distance with Galactic latitude, l. Still, further study and additional sky coverage of RRL in the SE region of Sgr may shed more light on this possibility.

7.2. *Dispersion*

As shown in Figure 9, the dispersion about the period-luminosity relation for the RRL in M 54 is on par with that of the RRL in Sgr. This would indicate a line-of-sight extent of over 2 kpc (Figure 8, whereas its on-sky

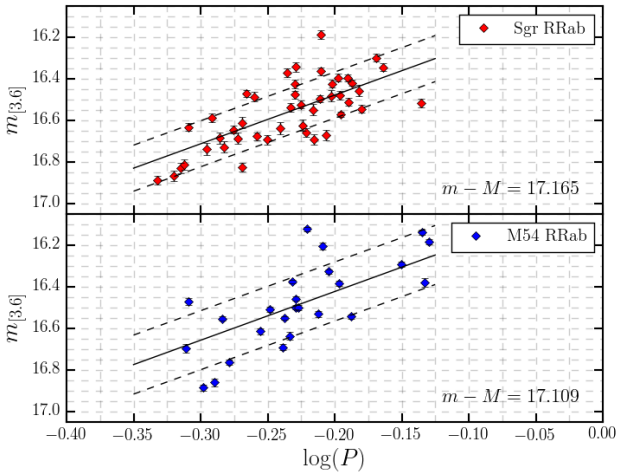

FIG. 9.— Period-luminosity relations at 3.6μm for (a) the RRL in Sgr (b) the RRL in M 54. Extinction-corrected mean, apparent magnitudes are plotted against log(P) in both panels. Solid black lines with slopes from the Neeley et al. (2017) period-luminosity relation are plotted over midpoint of the data. The dashed black lines represent 1σ uncertainties. The distance moduli of the two bodies are shown in the lower right of each panel.

radius of $r_t = 7.5$' translates to an width of just 58 pc at our measured distance. It is this highly unlikely that this is a physical 2 kpc extent rather than an effect of our data or methods. We suspect that this is an effect of crowding, which might still affect some of the stars in our gold sample. To better understand the source of the dispersion, we make an attempt to evaluate the level of crowding.

First, we performed several rounds of artificial star tests following the general procedures outlined by (Stetson & Harris 1988). We first generated a set of "artificial stars," consisting of an array of coordinate positions distributed across the cluster footprint and input magnitudes drawn randomly from a flat distribution between $m_{[3.6]} = 15.00$ and $m_{[3.6]} = 18.00$. We then transformed the input magnitudes to the raw DAOPHOT system by reversing the photometric calibrations discussed in §2.1. The artificial stars were then inserted into the cluster frames for each epoch using the ADDSTAR function in DAOPHOT and the corresponding, empirical model PSFs. Photometry was performed on the new, artificial images just as it was for the real images, with the exception that we adhered to the original PSFs rather than deriving new ones. We limited each round of tests to 150 artificial stars to avoid further inflating the level of crowding in the artificial images. Three rounds of tests were performed, and the inputs and outputs were then combined to create a more statistically robust sample.

In the absence of crowding, the input and output magnitudes of the artificial stars are expected to match, as they are generated and fit by the same model PSF and the pre- and post-photometry calibrations should negate each other. The output magnitude of an artificial star that is placed close to or on top of another star in the image, however, will likely deviate from the input. In addition, an artificial star placed in an extremely crowded or even saturated region of the image should not be detected at all.

We thus examine the artificial star detection rate and the difference between input and output magnitudes to determine how the RRL in our sample might be affected by crowding. It is important to note that this is not a strictly quantitative analysis, but rather a qualitative check on the RRL detection rates and photometry. Across all epochs, we find that the median detection rate drops steeply from 94% to 70% moving radially inward past the M 54 half-light radius ($r_h = 0.82$'). Of the artificial stars detected within the half-light radius, the median offset between input and output magnitude offsets was of the order $\Delta m = 1$, indicating that the photometry was very unreliable. These findings reflect the results of the initial photometry, for which no RRL were found to be accurately measured within 1' of the center of M 54. The median magnitude offset drops off exponentially with radius and falls to a steady $\Delta m = 0.1$ at roughly 3'. This is consistent with the poor RRL retention rate even at large radii. In addition, the ~ 0.1 mag median offset is consistent with the dispersion seen in Figure 9. We are therefore somewhat skeptical of the magnitude measurements for individual RRL, but we believe that the mean distance modulus and distance should hold up given the size of our sample.

7.3. *Metallicity Correction*

We note that neither the M 54 nor the Sgr measurements account for the metallicity dependence of the period-luminosity relation, which, although weaker in the infrared than in the optical (Catelan et al. 2004; Madore et al. 2013), is not insignificant (Neeley et al. 2017). Here, we make use of a known relation between optical RRL light curves and metallicities (Jurcsik & Kovacs 1996; Smolec 2005) to calculate [Fe/H] values for the M 54 RRL, then apply the 3.6μm period-luminosity-metallicity relation (Neeley et al. 2017) to derive a new distance modulus.

Jurcsik & Kovacs (1996) show that the metallicities of RRL are related to their periods and to one of the parameters, $\phi_{31} = \phi_3 - \phi_1$, of the Fourier sine series decomposition of their optical light curves. The ϕ_{31} values of the Fourier cosine decomposition for the RRL in our sample are provided in the the OGLE-IV catalog. We apply a $+\pi$ offset to these values to retrieve the parameters corresponding to the sine series. As determined by Smolec (2005), the individual metallicities can then be calculated as

$$[\mathrm{Fe/H}] = -3.142 - 4.902P + 0.824\phi_{31} \qquad (3)$$

We calculate [Fe/H] for each of the 25 RRL in our gold sample, then apply the 3.6μm period-luminosity-metallicity relation (Neeley et al. 2017) to calculate new absolute magnitudes. Again, we use the zero point derived by Benedict et al. (2011), yielding a new distance to M 54 of $d_{M54} = 24.93 \pm 0.34(\mathrm{ran}) \pm 0.92(\mathrm{sys})$ kpc. This distance places M 54 about 1.5 kpc closer than our initial result. We note, first, that this result is less precise, as additional uncertainties were introduced by incorporating metallicity information into the analysis. But the result should be more accurate, as it accounts for additional parameters that are known to influence the absolute luminosities of RRL. And such an offset is not unexpected, as Neeley et al. (2017) see a similar effect in comparing their period-luminosity and period-luminosity-metallicity relations for RRL in the globular

cluster M 4. This does indicate, however, that the metallicity cannot simply be ignored, as it is in the case of our Sgr distance result. Additional observations of the Sgr RRL to extract metallicities, either via spectroscopy or optical photometry, may allow for a more robust measurement of the separation of Sgr and M 54.

8. CONCLUSIONS

We present new, precise distance measurements to the core of the Sagittarius dwarf galaxy and to M 54 using photometry of *Spitzer* observations at 3.6μm. We take advantage of decreased line-of-sight extinction in the mid-infrared and incorporate a well-calibrated period-luminosity relation. We compare our result to previous Sgr distance measurements, noting that we are consistent with the most recent and most precise study to date by Hamanowicz et al. (2016). We provide a preliminary examination of the depth of Sgr, with a measured line-of-sight extension of several kiloparsecs, and propose a strategy of further analysis of the full three-dimensional structure of the core.

We also determine via the line-of-sight separation of M 54 and Sgr that Sgr has a cored dark matter halo. Our findings suggest that Sgr has undergone a cusp-core transformation, which is compatible with the rich star formation history and the dwarf galaxy.

We acknowledge support from a Virginia Space Grant Consortium Undergraduate Research Scholarship. A.F.G. would also like to thank members of the SMHASH collaboration, and particularly Vicky Scowcroft, for valuable advice, as well as staff at Carnegie Observatories for facilitating this research. This work is based on observations made with the *Spitzer Space Telescope*, which is operated by the Jet Propulstion Laboratory, California Institute of Technology under a contract with NASA.

REFERENCES

Alard, C. 1996, ApJ, 458, L17
Alcock, C., Allsman, R. A., Alves, D. R., et al. 1997, ApJ, 474, 217
Bellazzini, M., Ferraro, F. R., & Buonanno, R. 1999, MNRAS, 304, 633
Bellazzini, M., Ibata, R. A., Chapman, S. C., et al. 2008, AJ, 136, 1147
Benedict, G. F., McArthur, B. E., Feast, M. W., et al. 2011, AJ, 142, 187
Brooks, A. M., Papastergis, E., Christensen, C. R., et al. 2017, ApJ, 850, 97
Catelan, M., Pritzl, B. J., & Smith, H. A. 2004, ApJS, 154, 633
Cseresnjes, P., Alard, C., & Guibert, J. 2000, A&A, 357, 871
Goerdt, T., Moore, B., Read, J. I., Stadel, J., & Zemp, M. 2006, MNRAS, 368, 1073
Hamanowicz, A., Pietrukowicz, P., Udalski, A., et al. 2016, Acta Astron., 66, 197
Ibata, R., Lewis, G. F., Martin, N. F., Bellazzini, M., & Correnti, M. 2013, ApJ, 765, L15
Indebetouw, R., Mathis, J. S., Babler, B. L., et al. 2005, ApJ, 619, 931
Jurcsik, J., & Kovacs, G. 1996, A&A, 312, 111
Kunder, A., & Chaboyer, B. 2009, AJ, 137, 4478
Law, D. R., & Majewski, S. R. 2010, ApJ, 714, 229
Layden, A. C., & Sarajedini, A. 2000, AJ, 119, 1760
Madore, B. F., Hoffman, D., Freedman, W. L., et al. 2013, ApJ, 776, 135
Majewski, S. R., Skrutskie, M. F., Weinberg, M. D., & Ostheimer, J. C. 2003, ApJ, 599, 1082
Mashchenko, S., Wadsley, J., & Couchman, H. M. P. 2008, Science, 319, 174
Mateo, M., Mirabal, N., Udalski, A., et al. 1996, ApJ, 458, L13
Mateo, M., Udalski, A., Szymanski, M., et al. 1995, AJ, 109, 588
McDonald, I., Zijlstra, A. A., Sloan, G. C., et al. 2013, MNRAS, 436, 413
Monaco, L., Bellazzini, M., Ferraro, F. R., & Pancino, E. 2004, MNRAS, 353, 874
Monson, A. J., Beaton, R. L., Scowcroft, V., et al. 2017, AJ, 153, 96
Moore, B. 1994, Nature, 370, 629
Neeley, J. R., Marengo, M., Bono, G., et al. 2015, ApJ, 808, 11
—. 2017, ApJ, 841, 84
Persson, S. E., Madore, B. F., Krzemiński, W., et al. 2004, AJ, 128, 2239
Reach, W. T., Megeath, S. T., Cohen, M., et al. 2005, PASP, 117, 978
Schlafly, E. F., & Finkbeiner, D. P. 2011, ApJ, 737, 103
Schlegel, D. J., Finkbeiner, D. P., & Davis, M. 1998, ApJ, 500, 525
Scowcroft, V., Freedman, W. L., Madore, B. F., et al. 2013, ApJ, 773, 106
—. 2011, ApJ, 743, 76
Siegel, M. H., Dotter, A., Majewski, S. R., et al. 2007, ApJ, 667, L57
Siegel, M. H., Majewski, S. R., Law, D. R., et al. 2011, ApJ, 743, 20
Smolec, R. 2005, Acta Astron., 55, 59
Soszyński, I., Udalski, A., Szymański, M. K., et al. 2014, Acta Astron., 64, 177
Stetson, P. B. 1987, PASP, 99, 191
—. 1994, PASP, 106, 250
Stetson, P. B., & Harris, W. E. 1988, AJ, 96, 909
Teyssier, R., Pontzen, A., Dubois, Y., & Read, J. I. 2013, MNRAS, 429, 3068
Vera-Ciro, C., & Helmi, A. 2013, ApJ, 773, L4